Philosophical Magazine, 11 December 2003
Vol. 83, No. 35, 3977–3994

Taylor & Francis
Taylor & Francis Group

Development of new interatomic potentials appropriate for crystalline and liquid iron

M. I. Mendelev†, S. Han, D. J. Srolovitz

Princeton Materials Institute and Department of Mechanical and Aerospace Engineering, Princeton University, Princeton, New Jersey 08544, USA

G. J. Ackland

Department of Physics and Astronomy, University of Edinburgh, Edinburgh EH9 3JZ, UK

D. Y. Sun and M. Asta

Department of Materials Science and Engineering, Northwestern University, Evanston, Illinois 60091, USA

[*Received 20 May 2003 and accepted in revised form 7 August 2003*]

Abstract

Two procedures were developed to fit interatomic potentials of the embedded-atom method (EAM) form and applied to determine a potential which describes crystalline and liquid iron. While both procedures use perfect crystal and crystal defect data, the first procedure also employs the first-principles forces in a model liquid and the second procedure uses experimental liquid structure factor data. These additional types of information were incorporated to ensure more reasonable descriptions of atomic interactions at small separations than is provided using standard approaches, such as fitting to the universal binding energy relation. The new potentials (provided herein) are, on average, in better agreement with the experimental or first-principles lattice parameter, elastic constants, point-defect energies, bcc–fcc transformation energy, liquid density, liquid structure factor, melting temperature and other properties than other existing EAM iron potentials.

§1. Introduction

Atomistic computer simulations have played an important role in the development of our understanding of materials over the past 40 years. One key to accurate predictions of the structure and properties of material and their defects is the quality of the description of atomic interactions. The best existing approaches to describing atomic interactions in condensed phases are based on quantum-mechanical descriptions of bonding. Unfortunately, first-principles quantum-mechanical descriptions are computationally expensive and, hence, their application is usually limited to situations where the number of unique atoms is a few hundred

†Author for correspondence. Email: mendelev@princeton.edu.

Philosophical Magazine ISSN 1478–6435 print/ISSN 1478–6443 online
http://www.tandf.co.uk/journals
DOI: 10.1080/14786430310001613264

or (much) less. In addition, first-principles molecular dynamics (MD) simulation times rarely exceed a few picoseconds (Car and Parrinello 1988). Moreover, it should be noted that first-principles calculations of bonding in first-row magnetic transition metals (such as iron) are particularly difficult (and expensive). As a result, most large-scale and long-time atomistic simulations are performed using empirical or semiempirical descriptions of atomic interactions (Daw and Baskes 1984, Finnis and Sinclair 1984, Mehl and Papaconstantopoulos 1996). Such descriptions of atomistic interactions represent a compromise between computational efficacy, generality and accuracy.

Empirical potentials are commonly determined by fitting a proposed functional form to available data. These data may be obtained from either experimental measurements or first-principles calculations. Commonly, the input data include such quantities for perfect crystals as lattice parameter, cohesive energy, elastic constants and unrelaxed vacancy formation energy. Fitting potentials to data obtained only from perfect crystals has the disadvantage that the resultant fits can only be expected to be accurate for highly symmetric atomic configurations and situations in which the interatomic spacings are close to those in the equilibrium perfect crystal. This is a potential problem for applications that focus on crystal defects (such as interstitials, dislocations and grain boundaries), crystalline properties at high temperatures or the liquid. One approach to rectifying this deficiency is to fit the potentials also to properties that are sensitive to a wide range of atomic separations (especially small separations). Such properties include self-interstitial formation energies and the liquid structure factor. For example, relaxed self-interstitials in bcc crystals (figure 1), commonly exhibit interatomic spacings as small as three quarters of that of the nearest-neighbour spacing in the perfect crystal (Domain and Becquart 2001). Examination of the pair correlation function (PCF) of liquid or amorphous materials obtained from neutron or X-ray diffraction experiments (for example Waseda (1980)) also shows atom pairs at very small spacings. Approaches to fitting interatomic potentials using liquid state information have been proposed. For example, one is based upon a statistical mechanics relationship between parameters of an interatomic potential and liquid diffraction data (Mendelev and Srolovitz 2002) while another is based upon fits to atomic forces (obtained from first-principles calculations) in a proposed liquid structure (Ercolessi and Adams 1994).

In this paper, we examine several approaches to fitting interatomic potentials including fits to perfect crystal data, interstitial data and liquid data. These potentials are used to predict a range of material properties. The results of these calculations are then used to evaluate the efficacy of different fitting procedures. We limit this

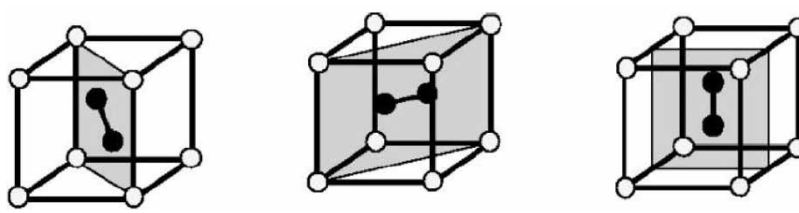

Figure 1. Schematic illustrations of the ⟨111⟩, ⟨110⟩ and ⟨100⟩ dumbbell interstitials in the bcc lattice.

study to interatomic potentials of the 'pair functional' form (Carlsson 1990), for example the embedded-atom method (EAM) (Daw and Baskes 1984), the Finnis–Sinclair (1984) potentials and the effective-medium theory (Jacobsen *et al.* 1987) for iron. This class of potentials was chosen because it has been successfully used to study a wide range of crystal and defect properties in metals and their alloys. Iron was chosen as the test case because iron-based materials are ubiquitous. There are several extant potentials of this type for iron (Johnson 1964, Pak and Doyama 1969, Osetsky *et al.* 1995, Ackland *et al.* 1997, Lee *et al.* 2001). However, no single potential of this form is completely satisfactory for describing a wide range of defects in crystals and the liquid structure. The potentials described by Johnson (1964), Pak and Doyama (1969) and Osetsky *et al.* (1995) are purely pairwise and, therefore, cannot provide an adequate description of elastic and defect properties in metals. The EAM potential (Ackland *et al.* 1997) will be considered in detail in the next section. Although the potential developed by Lee *et al.* (2001) explicitly incorporates angular contributions within the modified embedded-atom method (MEAM) formulation (Baskes 1992, Lee and Baskes 2000), it does not provide an accurate prediction of either the melting point (2200 K calculated versus 1812 K measured) or the interstitial formation energy (4.23 eV from MEAM versus 3.41 eV from the first-principles calculations of Domain and Becquart (2001)). Therefore the necessity to develop a new simple empirical potential for iron is clear.

§ 2. Potentials fitted to perfect crystal properties alone

We begin by examining one of the widely used EAM potentials for iron that was fitted to perfect crystal properties (Ackland *et al.* 1997). The total potential energy in the EAM is divided into two contributions, namely a pairwise part and a local density part:

$$U = \sum_{i=1}^{N-1} \sum_{j=i+1}^{N} \varphi(r_{ij}) + \sum_{i=1}^{N} \Phi(\rho_i), \tag{1}$$

where the subscripts i and j label distinct atoms, N is the number of atoms in the system, $r_{i,j}$ is the separation between atoms i and j and

$$\rho_i = \sum_j \psi(r_{ij}). \tag{2}$$

All functions given by Ackland *et al.* (1997) were represented as sums of basis functions:

$$\varphi(r) = \sum_{k=1}^{n^{\varphi}} a_k^{\varphi} \varphi_k(r), \tag{3}$$

$$\psi(r) = \sum_{k=1}^{n^{\psi}} a_k^{\psi} \psi_k(r), \tag{4}$$

$$\Phi(\rho) = \sum_{k=1}^{n^{\Phi}} a_k^{\Phi} \Phi_k(\rho), \tag{5}$$

where ϕ_k, ψ_k and Φ_k are the basis functions and a_k are coefficients to be fitted to material properties. Different basis functions (e.g. cubic splines, exponentials and polynomials) have been used in the literature (for example Ackland *et al.* (1997)). While only a single basis function ($n^{\Phi}=1$ with $\Phi_1(\rho)=-\rho^{1/2}$ and $a_1^{\Phi}=1$) was used for the embedding energy Φ in the work of Ackland *et al.* (1997), equation (5) provides a more general form that will be used in the present development. Note that the Finnis–Sinclair and the EAM potentials for single-component systems are essentially identical, with the exception of the form of the embedding energy function employed (Finnis and Sinclair represent it as a square root and it is represented in the EAM by a general function, to be determined). Because of this similarity, we refer to both classes of potentials by the same term: EAM potentials.

The coefficients of this potential were chosen to fit the lattice parameter, cohesive energy, unrelaxed vacancy formation energy and elastic constants for α-Fe at $T=0$. Although Ackland *et al.* (1997) did not have the quantitative data for the interstitial formation energy in pure iron, they adjusted the potential to ensure that the $\langle 110\rangle$ dumbbell was the most stable interstitial configuration, as suggested by experiment. Several physical properties determined with this potential are given in table 1. This potential yields good agreement with empirical universal p–V relations derived by Rose *et al.* (1984) and the universal binding energy relations down to $0.85a/a_0$, where a_0 is the equilibrium lattice parameter in bcc iron at $T=0\,\mathrm{K}$ (figure 2).

The ability of this potential to describe the system accurately at high densities and the proper interstitial configuration suggests that this potential is suitable for simulating atomic configurations and properties with small atomic separations. To test this supposition, we used MD to simulate liquid iron. Unless otherwise noted, all liquid iron simulations were performed at $T=1820\,\mathrm{K}$ with 5000 atoms in the NVT ensemble. The structure factor $S(K)$ obtained from these simulations (using the PCF up to 2 nm) with this EAM potential (figure 3) shows rather poor agreement with the experimental data from (Il'inskii *et al.* 2002) (note that the error in determining the structure factor from the simulation is less than 0.1 at the position of the first peak). Given that the first peak of the structure factor is significantly higher than in experiment, we suspect that this EAM potential provides a liquid structure that is more ordered than observed (Mendelev 1999). The same conclusion can be made from figure 4, which demonstrates that the potential developed by Ackland *et al.* (1997) greatly overestimates the first peak of the PCF $g(r)$ relative to experiment (Il'inskii *et al.* 2002). Nonetheless, this potential provides reasonable values for the bcc lattice parameter, the latent heat at 1820 K and the $\{100\}$ surface energies of bcc iron at $T=0\,\mathrm{K}$ (see table 1).

To find the melting point corresponding to the EAM potential from the paper by Ackland *et al.* (1997), we performed a series of simulations based on the so-called coexistence approach (Morris *et al.* 1994, Morris and Song 2002). We begin by performing simulations of bulk bcc iron to determine the crystalline lattice parameter as a function of temperature. Subsequently, we set up a simulation box initially containing $10\times10\times50$ bcc unit cells with a lattice constant corresponding to the temperature, representing our initial estimate of the melting point. Half of the atoms are subsequently melted, leading to a periodic simulation cell containing two solid–liquid interfaces. The velocities of the particles in this simulation cell are subsequently reinitialized at our estimated value of the melting point, and MD simulations are then performed employing Parinello–Rahman (1980, 1981, 1982) dynamics with the length of the simulation cell normal to the interfaces dynamic

Table 1. Physical properties calculated with the EAM potentials. The properties used in the fitting procedure are printed in bold.

Property	Target value	Value for the following potentials: Johnson (1964) potential	Ackland *et al.* (1997) potential	Potential 1	Potential 2	Potential 3	Potential 4	Potential 5
a (Å), bcc at $T=0$ K	2.8553[a]	2.8600	2.8665	**2.8553**	**2.8553**	2.8823	**2.8557**	**2.8553**
a (Å), bcc at $T=1820$ K	2.94	2.965	2.921	2.922	2.926	–[b]	2.930	2.908
E_{coh} (eV atom^{-1}), bcc	−4.316[a]	−1.537	−4.316	−4.126	−4.122	−5.170	−4.155	−4.134
E_f^v (eV), bcc at $T=0$ K	1.84[a]	1.54	1.89	**1.84**	**1.84**	2.72	**1.87**	**1.85**
E_D (eV atom^{-1}), bcc at $T=0$ K	2.65[b]	2.05	2.49	2.40	2.34	2.08	2.24	2.24
E_f^i (eV), ⟨100⟩ bcc at $T=0$ K	4.37[d]	5.93	6.12	3.92	**4.34**	3.08	3.77	**4.33**
E_f^i (eV), ⟨110⟩ bcc at $T=0$ K	3.41[d]	4.64	4.88	3.46	**3.53**	2.40	3.20	**3.50**
E_f^i (eV), ⟨111⟩ bcc at $T=0$ K	4.11[d]	4.90	5.02	3.67	**4.02**	2.63	3.52	**3.93**
C_{11} (GPa), bcc at $T=0$ K	243.4[a]	192.3	243.4	**243.4**	**243.4**	143.7	**243.5**	**243.7**
C_{12} (GPa), bcc at $T=0$ K	145.0[a]	96.1	145.0	**145.0**	**145.0**	87.5	**145.0**	**145.1**
C_{44} (GPa), bcc at $T=0$ K	116.0[a]	96.1	116.0	**116.0**	**116.0**	41.3	**115.8**	**115.9**
γ_{100} (eV Å^{-2}), bcc at $T=0$ K	0.136[e]	0.079	0.113	0.105	0.110	0.183	0.125	0.140
a (Å), fcc at $T=0$ K	3.6583[e]	3.7005	3.6800	**3.6581**	**3.6584**	3.6454	**3.6522**	**3.6583**
$\Delta E_{bcc\rightarrow fcc}$ (eV atom^{-1})	0.122[e]	0.027	0.054	**0.120**	**0.120**	0.049	**0.127**	**0.119**
ρ_{liquid} (GPa), $T=1820$ K	0.00[f]	5.434	−0.460	−1.173	**−0.034**	**0.031**	**0.006**	**−0.006**
PCF first peak position (Å), $T=1820$ K	2.49[g]	2.51	2.53	2.48	2.48	**2.49**	**2.48**	**2.50**
PCF first peak height, $T=1820$ K	2.28[g]	2.80	2.87	2.43	2.46	**2.30**	**2.36**	**2.42**
D_{liquid} (10^{-5} cm^2 s^{-1}), $T=1820$ K		1.61	1.19	3.34	3.62	4.66	4.37	3.60
ΔH_{melt} (eV atom^{-1}), $T=1820$ K	0.143	0.115	0.188	0.186[h]	0.162	—	0.153	0.187
R_{F1} (eV Å^{-1})	0.00	0.61	0.63	**0.24**	**0.27**	1.57	1.49	1.49
R_{F2} (eV Å^{-1})	0.00	0.69	0.66	0.25	0.28	1.15	1.08	1.06

[a]These values were from Ackland *et al.* (1997). See Ackland *et al.* (1997) for the original references.
[b]The crystal melts much below $T=1820$ K.
[c]Gardner *et al.* (1968).
[d]Domain and Becquart (2001).
[e]First-principles calculations performed as part of this work.
[f]The pressure was calculated at the experimental density, 0.076 atom Å^{-3} (Waseda 1980).
[g]Il'inskii *et al.* (2002).
[h]This value is determined at the experimental density.

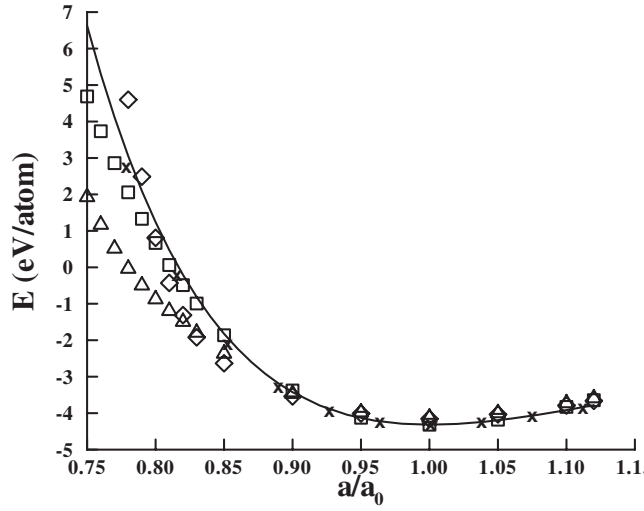

Figure 2. The internal energy versus lattice parameter at $T = 0\,\mathrm{K}$, where a_0 is the zero-pressure lattice parameter: (——), universal binding energy relation; (□), data obtained using the Ackland *et al.* (1997) potential; (△), data obtained using potential 2; (◇), data obtained using potential 4; (×), data obtained using first-principles calculations. Note that the fitting procedures used to obtain these potentials did not use any atomic configurations for which the minimum interatomic separation was less than $0.82a_0$.

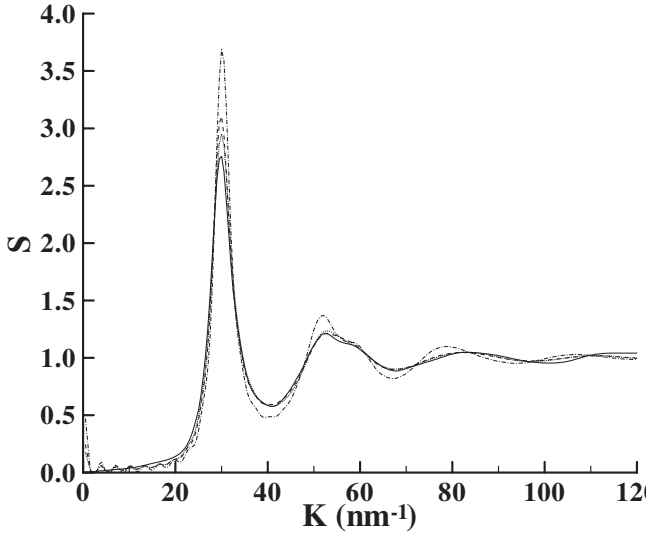

Figure 3. Structure factor for iron at 1820 K: (——), experimental data (Il'inskii *et al.* 2002); (– · –), MD simulations using the Ackland *et al.* (1997) potential; (- - -), MD simulations using potential 1; (· · · · · ·), MD simulations using potential 2.

(to yield zero average normal stress) and the dimensions parallel to the interfaces fixed. A refined estimate of the melting point is then derived from the average temperature measured from such a coexistence simulation. The dimensions of the simulation cell are then adjusted according to the lattice constant of the crystal

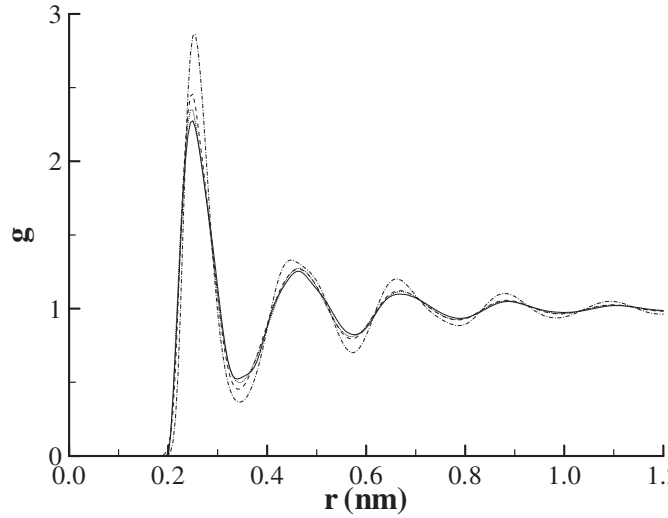

Figure 4. Pair correlation function for iron at 1820 K: (——), experimental data (Il'inskii *et al.* 2002); (– · –), MD simulations using the Ackland *et al.* (1997) potential; and 4 (dotted line).

Table 2. Liquid–solid transformation properties.

	T_{melt} (K)	ΔH_{melt} (eV atom^{-1})	ΔV_{melt} (Å^3 atom^{-1})
Experiment	1812	0.143	0.38
Ackland *et al.* (1997) potential	2358	0.218	0.81
Potential 2	1772	0.162	0.62
Potential 4	1753	0.157	0.59

at this new temperature, and the procedure iterated until the coexistence temperature is derived corresponding to zero values of the stresses in the bulk crystal and liquid phases. The final coexistence temperature is used as our prediction of the zero-pressure melting temperature. In addition, the latent heat and the change in volume associated with melting were determined. These results are presented in table 2. Examination of these data demonstrates that this EAM potential (Ackland *et al.* 1997) overestimates the melting point by more than 500 K and yields an unreasonably large change in volume upon melting.

One of the properties to which the potential given by Ackland *et al.* (1997) was fitted is the cohesive energy. This is routinely done in order to set the energy scale of the potential and in order to fit the universal binding energy relation (which was necessary to provide the correct behaviour of the potential at small atomic separations). Examination of the data presented in tables 1 and 2 and figure 3 shows that fitting to the universal binding energy relation does not ensure accurate prediction of properties (e.g. interstitial formation energy and latent heat) involving small interatomic separations. For example, the formation energy of bcc interstitials are predicted to be more than 1 eV larger than values obtained from first-principles calculations. Also, it is important to note that the liquid PCF obtained with the EAM potential from the work of Ackland *et al.* (1997) at

$T = 1820$ K shows atoms as close together as 0.2 nm ($0.85a_0$), approximately the same minimum separation as found in the interstitial dumbbells. While the EAM potential is shown in figure 2 to produce accurate energy–volume relations for the bcc structure down to these small interatomic separations, it leads to large discrepancies with experiment in the prediction of the liquid PCF (figure 4). In particular, the first peak height is overestimated by this potential. This result and the overestimation of interstitial formation energies indicate that the interatomic interactions predicted by the EAM potential given by Ackland *et al.* (1997) are too repulsive at small separations. On this basis we conclude that fitting to the universal binding energy relation, and thus the cohesive energy, does not ensure an accurate description of interatomic forces over a wide range of coordination and bond length.

Table 1 also exhibits the same set of material properties obtained with a classical pair potential for iron, that is the well-known Johnson (1964) potential. It is interesting to note that this pair potential gives reasonable values for most properties, but (as pair potentials must) yields $C_{12}=C_{44}$ and the unrelaxed vacancy formation energy is equal to the cohesive energy.

§ 3. Potentials fitted to first-principles forces

In the previous section, we demonstrated that fitting EAM-type potentials solely to perfect crystal properties is insufficient to reproduce properly such important properties as the liquid structure factor and the interstitial formation energy. In this section, we expand the set of properties included in the fit to include atomic forces, obtained from first-principles calculations, as originally was proposed by Ercolessi and Adams (1994). We use the following approach: we generate a crude atomic model for a liquid of the correct density, perform a first-principles calculation of the forces on all atoms within this model and use these to fit potential parameters. The procedure ensures consideration of a range of atomic geometries, including cases of small atomic separations in asymmetric configurations.

In the present work we created the initial liquid model by running a MD simulation using a very simple pair potential taken from the work of Pak and Doyama (1969) at $T = 1820$ K and the experimental density, 0.076 atom Å^{-3} (Waseda 1980). Although the resultant liquid structure may be far from the experimental structure, it does provide the requisite range of atomic configurations in a liquid-like structure of the correct density. The first-principles computations were performed using the pwscf code (Baroni *et al.* 2003). An ultrasoft pseudopotential (Vanderbilt 1990) was employed to describe electron–ion interactions while the electron–electron interactions are described in the generalized gradient approximation (Perdew *et al.* 1996). A plane-wave basis set with an energy cut-off of 30 Ry was employed. We included spin polarization to address the correlation of the local moment of iron atoms. The temperature effect was considered through the finite-temperature formulation of Kohn–Sham theory (Mermin 1965) where electron occupations are determined from the Fermi–Dirac formula with a temperature of 1850 K. Since the first-principles calculations require substantial computational time, the liquid models were limited to only 100 atoms. According to the first-principles calculation, the maximum and average total forces acting on an atom are 3.85 and 1.03 eV Å^{-1} respectively.

The three components of the force vectors on each of the N atoms obtained from the first-principles calculations provide $3N$ additional equations that can be used to

fit the coefficients in front of the basis functions (i.e. $a_k^{\varphi}, a_k^{\psi}$ and a_k^{Φ}) in the various terms of the potential:

$$\begin{aligned} F_{ix}\left(a_k^{\varphi}, a_k^{\psi}, a_k^{\Phi}\right) &= F_{ix}^{\mathrm{fp}}, \\ F_{iy}\left(a_k^{\varphi}, a_k^{\psi}, a_k^{\Phi}\right) &= F_{iy}^{\mathrm{fp}}, \\ F_{iz}\left(a_k^{\varphi}, a_k^{\psi}, a_k^{\Phi}\right) &= F_{iz}^{\mathrm{fp}}, \end{aligned} \tag{6}$$

where the forces on atom i on the left-hand side are calculated using equations (1)–(5) and those on the right-hand side are obtained from the first-principles calculations. The coefficients in the potential are determined by minimizing the deviations between the first-principles and potential forces together with those of any other physical property that is available, that is

$$R^2 = R_{\mathrm{F}}^2 + \sum_{\alpha=1}^{A} \lambda_\alpha (P_\alpha - P_\alpha^{\mathrm{o}})^2,$$

where P_α and P_α^{o} label each of the A properties included in the fitting procedure as determined using the potential and some other trusted means (i.e. experiment or first-principles) respectively, and R_{F} is the deviation between the first-principles forces and those obtained from the potential:

$$R_{\mathrm{F}}^2 = \frac{1}{3N} \sum_{i=1}^{N} \left[\left(F_{ix} - F_{ix}^{\mathrm{fp}}\right)^2 + \left(F_{iy} - F_{iy}^{\mathrm{fp}}\right)^2 + \left(F_{iz} - F_{iz}^{\mathrm{fp}}\right)^2 \right]. \tag{7}$$

The fitting is done in the following manner. Firstly, we make use of the fact that all properties are linear functions of the coefficients in front of the basis functions in the pairwise $\{a_k^{\varphi}\}$ and embedding $\{a_k^{\Phi}\}$ energy terms of the EAM potential. Therefore, we start with an initial guess for the coefficients in front of the basis functions of the density function $\{a_k^{\psi}\}$ and determine $\{a_k^{\varphi}\}$ and $\{a_k^{\Phi}\}$ using a least-squares fit. Next, we use a gradient search method to obtain the new $\{a_k^{\psi}\}$ and iterate to convergence. At this stage, we fit to the following properties:

(i) first-principles forces;
(ii) lattice parameters of bcc and fcc iron at $T = 0\,\mathrm{K}$;
(iii) bcc cohesive energy;
(iv) unrelaxed bcc vacancy formation energy;
(v) energy difference between bcc and fcc crystals.

All target values for these properties are shown in table 1. The next stage of the fitting procedure is to fix the coefficients $\{a_k^{\psi}\}$ at the values obtained from the minimization described above and further to refine the coefficients $\{a_k^{\varphi}\}$ and $\{a_k^{\Phi}\}$ by fitting to additional sets of properties, as described below. In this refinement stage, we no longer force the potential to match the cohesive energy for the reasons outlined in the previous section.

In the first refinement case, which we refer to as EAM potential 1, the pairwise and embedding energy functions were fitted to the three elastic constants of bcc iron, in addition to the standard set of properties:

(i) first-principles forces;
(ii) lattice parameters of bcc and fcc iron at $T = 0\,\mathrm{K}$;

(iii) unrelaxed bcc vacancy formation energy;
(iv) energy difference between bcc and fcc crystals.

The main difference between this potential and that derived by Ackland *et al.* (1997) is that in the present case we also fit to the first-principles forces in a liquid-like structure. Both the fitted properties and a series of properties, which were not used in the fitting procedure are shown in table 1. These data demonstrate that potential 1 yields a more accurate prediction of the interstitial formation energy (in comparison with a first-principles calculation (Domain and Becquart 2001)) than does the original potential (Ackland *et al.* 1997) (even though this was not in the fit). This improvement can be attributed to the fact that the new potential was fitted to first-principles forces in a liquid-like configuration and that both interstitials and liquids contain smaller atomic separations than occur in a perfect bcc iron crystal. Note that the liquid structure employed in the fitting procedure was not the real iron liquid structure, but rather a very crude approximation. In order to test the sensitivity of the new potential to the detailed liquid structure, we created a liquid model using the new potential 1. The structure factor of the resultant liquid is shown in figure 3. Clearly, this structure factor is in much better agreement with the experimental data than that obtained with the Ackland *et al.* (1997) potential. Note (see table 1) that the pressure in this liquid model is not zero (this corresponds to a liquid density 1.6% larger than in experiment). Although the cohesive energy was excluded from the second stage of the fitting procedure, potential 1 still provides a reasonable value of the cohesive energy at $T = 0\,\mathrm{K}$ (only a 5% deviation from the target value). Furthermore, it gives approximately the same latent heat and the {100} bcc surface energy as the Ackland *et al.* (1997) potential, which was forced to match exactly the cohesive energy (see table 1). These results suggest that there is no need to fit the cohesive energy in order to obtain crystal and crystal defect properties.

Although potential 1 yields reasonable values for the interstitial formation energy, the deviation with respect to the first-principles results is too large for some applications (e.g. radiation damage simulations). The liquid density predicted using potential 1, while reasonable, differs from the experimental value by more than the uncertainty in the experimental measurement. In order to address these deficiencies, we expand our fit to include the interstitial formation energies and the liquid density, yielding potential 2. The complete description of this potential can be found in appendix A. It is interesting that the addition of the interstitial formation energies and liquid density to the fitting procedure yielded some improvement in the agreement with the experimental structure factor (see figure 3). The properties associated with this new potential are compared with the target properties in table 1. In addition, table 2 shows the melting point, latent heat and change in volume upon melting obtained with this potential and from experiment. These results show that the predicted melting point differs from the experimental value by only 40 K. Since the melting point was not used in the fitting procedure, such agreement can be considered as satisfactory. While the new potential 2 yields melting properties that are in much better agreement with the experimental measurements than does the Ackland *et al.* (1997) potential, the agreement is still not ideal (recall, however, that none of these properties was included in the fit).

Both potential 1 and potential 2 were fitted to the first-principles total forces calculated over the same 'liquid' atomic configuration. Examination of the value of R_{F1} in table 1 shows that we were able to fit the first-principles forces to within only

approximately 25% in the two cases. Note, however, that this is a vast improvement over the predictions obtained using the earlier EAM potential (see table 1). The total forces to which we fit were obtained for a single small liquid-like model. It is of interest to inquire how well we can reproduce the forces for another liquid-like structure. As an example, such a structure was created to be consistent with the experimental liquid iron diffraction data using the method described by Mendelev (1999). The first-principles forces obtained for this model showed maximum and average values of 4.38 and 0.98 eV Å^{-1} respectively. A comparison of the rms deviation of these forces R_{F2} from those obtained using the different potentials, is shown in table 1. Examination of these data shows that an EAM potential fitted to the first-principles forces from one particular liquid configuration provide approximately the same level of agreement with the first-principles forces from another liquid configuration.

In the EAM formalism, a positive second derivative of the embedding function ($\Phi''(\rho) > 0$) ensures that the potentials give rise to increases in bond strength resulting from a reduction in coordination (Carlsson 1990). As reviewed by Carlsson (1990), this effect is known to underlie a number of important features of defect properties in metals. It is thus important to point out that in this work we used the following form of the embedding function: $\Phi(\rho) = -\rho^{1/2} + a^{\Phi}\rho^2$ (see appendix A) and obtained a negative value of a^{Φ}. Since $\Phi''(\rho)$ must be positive, it is clear that the resultant potential becomes unphysical when $\rho > \rho_c = [-1/(8a^{\Phi})]^{2/3} \approx 50$. In all the atomic configurations we examined in our fitting procedure, the value of ρ is much smaller than this critical value. For example, in perfect bcc iron with the equilibrium lattice parameter, $\rho = 26.3$. In the case of a $\langle 100 \rangle$ interstitial in bcc iron, the maximum value of ρ was found to be $\rho_{max} = 30.7$. Finally, the maximum value of ρ in a liquid model was $\rho_{max} \approx 30$ at $T = 1820$ K and $\rho_{max} = 33$ at $T = 2200$ K. Clearly, our fitting procedure cannot be expected to provide the correct behaviour of the embedding energy functions for values of ρ larger than those involved in the fitting (i.e. $\rho > 33$ in the present case).

Note that, in all cases in our models where small atomic separations were observed, no atom had more than three neighbours that were located at very small distances (much smaller than in the equilibrium crystal). Hence, under normal circumstances the values of ρ that are likely to be encountered do not differ too much from those in the equilibrium crystal. On the other hand, if we consider a perfect crystal, hydrostatically compressed to the same minimum distances seen in the liquid or defected crystal, the situation would be quite different. In this case, all the nearest-neighbour distances are simultaneously very small and, correspondingly, ρ is very large. For example, if a crystal was compressed such that its lattice parameter was 95% of that in the zero-pressure crystal ($a/a_0 = 0.95$), $\rho = 33.5$ for potential 2. This is equivalent to the maximum value of ρ found in a liquid at $T = 2200$ K using the same potential. It is interesting, that potential 2 provides good agreement with up to $a/a_0 = 0.95$. While the agreement between potential 2 and the universal binding energy relation predictions is poor for $a/a_0 < 0.95$, first-principles and universal binding energy relation predictions are in good agreement down to very small values of a/a_0. The disagreement between potential 2 and the universal binding energy relation predictions observed for $a/a_0 < 0.95$ can be explained by the fact that the uniform deformation assumed in the universal binding energy relation at these lattice parameters gives ρ values much larger than in any of our models. This demonstrates why fitting the potential at small atomic separations to the

universal binding energy relation does not yield better predictions of the liquid structure or the interstitial formation energies. Conversely, potential 2 should not be applied in cases of very large homogeneous deformations (see figure 2).

Just as potential 2 is not expected to be useful at very large ρ (e.g. greater than 33), we should also expect that the potential is not useful when ρ is much smaller than those sampled in the configurations to which this potential was fitted. The smallest value of ρ found in the liquid model at $T = 1820\,\mathrm{K}$ is $\rho_{\min} = 14$. This is the limit below which the potential cannot be expected to provide reliable information. Indeed, examination of table 1 shows that the $\langle 100 \rangle$ surface energy of bcc iron, where $\rho_{\min} = 15$, calculated with potential 2 is 20% smaller than that obtained from first-principles calculations.

E_f^v in table 1 is the unrelaxed vacancy formation energy, that is the difference between the energy of a perfect crystal with one atom removed (and all other atomic positions fixed) and $N\varepsilon_0$, where N is the number of atoms in the crystal with a vacancy and ε_0 is the energy per atom in the perfect crystal. While it is convenient to use this value in the fitting procedure, it clearly must differ from the experimental vacancy formation energy (where the atom positions are relaxed). Therefore, the target vacancy formation energy in table 1 was obtained using first-principles calculations of an unrelaxed crystal with a single vacancy. The relaxed vacancy formation energy can be obtained by minimizing the total energy of the system with a vacancy with respect to the atomic coordinates.

Experimental data are available for the activation energy E_D for self-diffusion, which is the sum of the relaxed vacancy formation energy and the vacancy migration energy (Shewmon 1963). To find the migration energy, we examine the energy of a crystal with a single vacancy as we translate an atom (one of the atoms that is a nearest neighbour of the vacancy) in a straight line drawn from its original relaxed position to its relaxed position after it exchanged with the vacancy. The energy versus distance is shown in figure 5; the minimum of this plot is the relaxed vacancy

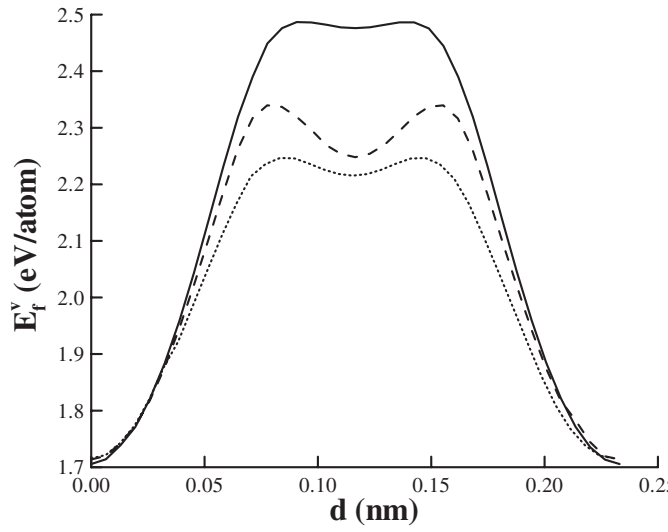

Figure 5. The vacancy energy versus displacement d along the [111] direction obtained with the Ackland *et al.* (1997) potential (——), potential 2 (- - -) and potential 4 (· · · · · ·).

formation energy and the difference between this and the activation for diffusion is the maximum of this plot (the migration energy is simply the difference between these two). The maximum or activation barrier does not occur at the midpoint but is rather slightly displaced from the midpoint in either direction. Such a double-humped energy landscape is also observed in calculations with the EAM potential (Ackland *et al.* 1997). The activation energy for diffusion is quoted in table 1. Potential 2 and the Ackland *et al.* potential (1997) give approximately the same value, which is within approximately 10% of the experimental measurement.

§4. Potentials fitted to the liquid structure factor

Another approach to the incorporation of small atomic separation information into the fitting procedure is through the direct use of experimental liquid structure data. The structure factor for liquid iron near the melting point was obtained by Il'inskii *et al.* (2002). The Fourier transformation of the structure factor leads to the PCF, which we use here. A more complete description of the procedure of fitting potentials to PCF data has been given by Mendelev and Srolovitz (2002). In this procedure, we employ the function $\psi(r)$ obtained as described in the previous section (fit only to lattice parameters, cohesive energy, unrelaxed vacancy formation energy and the relative bcc and fcc energies) and only refitted the pairwise energy function φ and embedding energy function Φ. Firstly, we fitted potential 3 to only the PCF and the liquid density. Figure 6 demonstrates that the fitting procedure provides excellent agreement between the model and experimental structure factor. To refine this potential further, we added the bcc and fcc lattice parameters, the bcc unrelaxed vacancy formation energy and the bcc→fcc transition energy, and all three elastic constants of the bcc iron to the fitting procedure to generate potential 4 (see appendix A for a complete description of this potential). The addition of the perfect crystal properties at $T=0\,\mathrm{K}$ led to a slight worsening of the agreement

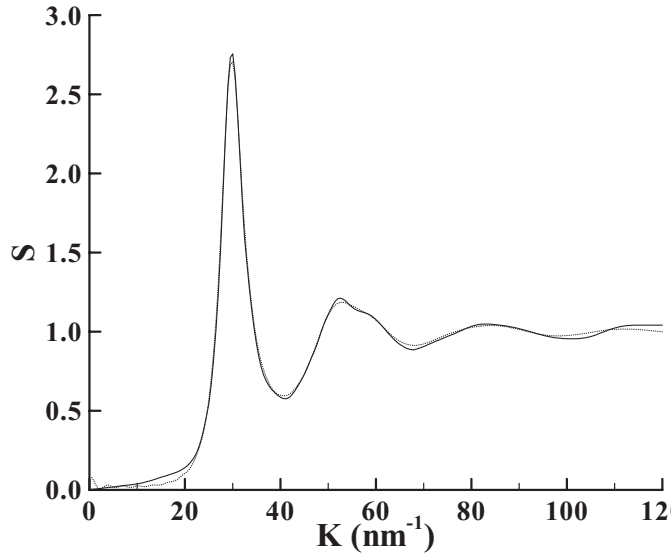

Figure 6. Structure factor for iron at 1820 K: (——), experimental data (Il'inskii *et al.* 2002); (· · · · · ·), potential 3.

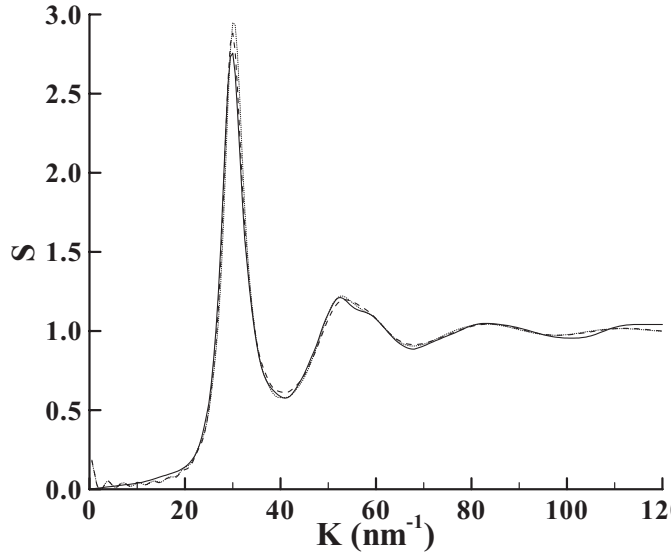

Figure 7. Structure factor for iron at 1820 K: (——), experimental data (Il'inskii *et al.* 2002); (- - -), MD simulations using potential 4; (· · · · · ·), MD simulations using potential 5.

with the experimental structure factor (see figure 7). Tables 1 and 2 demonstrate that inclusion of the liquid structure factor information in potential 4 provides more accurate values of the surface energy in bcc iron at $T = 0$ K, latent heat of melting and volume change than does potential 2, although slightly worse values for the melting temperature and the activation energy for self-diffusion in bcc iron. However, all these differences are rather small and we can conclude that both fitting procedures used to generate the potentials lead to nearly the same properties. Examination of figure 8 shows that both procedures produce nearly the same potential. This suggests that improving the short-range behaviour of the potentials using first-principles forces in a liquid-like structure and directly including the experimental liquid diffraction data are nearly equivalent.

Table 1 shows that potential 4 does not yield accurate interstitial formation energies. The interstitial formation energies are extremely sensitive to small changes in the interatomic potential. This may be traced to the relatively small interatomic separation in bcc interstitials, which in turn gives rise to large (and highly anisotropic) and long-range elastic relaxations. Given the nature of these relaxations, errors of order 0.5 eV in the interstitial formation energy are not surprising. To address the interstitial formation energy errors resulting from potential 4, we have refitted this potential to include also the interstitial formation energy: potential 5. This led to a small decrease in the agreement with the experimental structure factor (see figure 7) but, on the other hand, greatly improved the agreement with the first-principles interstitial formation energy.

It is notable, but not surprising, that the potentials fitted to liquid structure factor data yield worse agreement with the first-principles forces for the liquid-like structure, as seen in table 1. In fact, the values of R_F for potentials 4 and 5 are even larger than the mean forces on the atoms in the system. It is not clear how this will affect the dynamic behaviour of this material. Table 1 shows that the effect of these

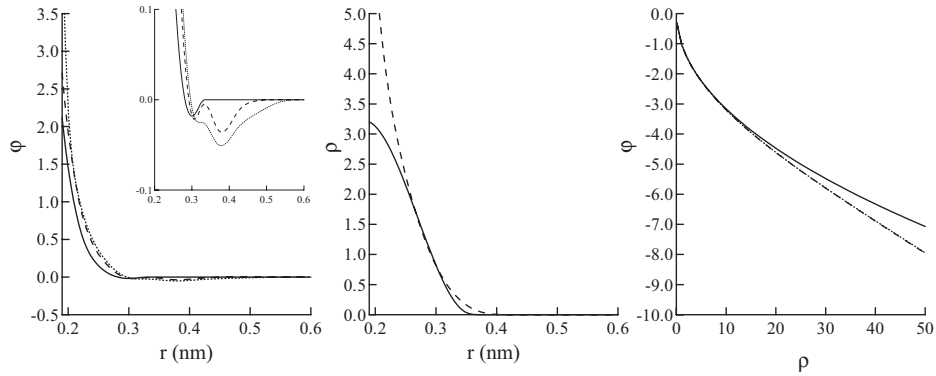

Figure 8. EAM potentials: (——), Ackland *et al*. (1997); (- - - -), potential 2; (· · · · · ·), potential 4.

errors is minimal on the kinetic parameters that we examined in the present work (i.e. the activation energy for self-diffusion in bcc iron and the diffusivity in the liquid state); cf. the same parameters obtained using potential 2 for which R_F is small.

§ 5. Discussion and conclusions

Two procedures were developed to fit the EAM potentials in the present work. While both procedures use the perfect crystal data and crystal defect information, the first procedure also uses first-principles forces to obtain the proper pairwise part behaviour at small atomic separations and the second procedure uses experimental diffraction data for the same purposes. The advantage of the first procedure is related to the fact that the diffraction data are not always available. In addition, while the accuracy of the first-principles calculation certainly will improve with increases in computer power and further advances in first-principles calculations, there is no reason to expect concomitantly large improvements in the accuracy of the diffraction data. The reliability of the diffraction data for our application is further compromised by the fact that we actually use pair correlation function data rather than the structure factor and the structure factor is only measured over a finite range (the Fourier transformation formally requires knowledge of $S(K)$ from 0 to ∞). The advantage of the second (diffraction data) procedure is that it yields potentials for which the MD simulation data are in good agreement with the experimental diffraction data. In the case of pure iron, the agreement between $S(K)$ predicted using the potential obtained using the first procedure and the experimental data is only slightly worse than when the second procedure is employed. There is, however, no guarantee that the first procedure will work so well for other systems. For example, the procedure used to fit an EAM potential for pure aluminium used by Ercolessi and Adams (1994) is very similar to our first procedure but yields relatively poor agreement between predicted and measured structure factors (J. R. Morris 2003, private communication). This is despite the fact that this potential (Ercolessi and Adams 1994) provides excellent agreement with the melting point and latent heat. Clearly, the failure to predict properly the liquid structure can be of great consequence when such a potential is used for simulating solid–liquid interface properties. It is important to note that the good reproduction of the liquid structure usually provides a correct value of diffusivity (for example Mendelev (1998a,b)).

Examination of table 1 shows that all potentials developed in this work (even potential 3 which provides poor agreement with the target values for most properties) give about the same diffusivity, while for example the Johnson (1964) and Ackland *et al.* (1997) potentials, which lead to a much higher first peak in the PCF, also yield diffusivities that are much too small. Since potential 2 provides reasonable agreement with both the experimental diffraction data and the first-principles forces, we recommend using this potential in simulations of defects in bcc iron and for the solid–liquid interface properties. The parameters of this potential are given in appendix A.

An alternative to trying to incorporate the effects of small atomic separations through liquid diffraction or force data is to fit the potential using the universal binding energy relation. For example, the pairwise term in the potential described by Lee *et al.* (2001) is determined from the difference between the energy predicted by this universal relation and the embedding term. Our results and those of Lee *et al.* (2001) show that this method does not produce reasonable liquid structures nor interstitial formation energies. The point is that small atomic separations are incorporated into the universal binding energy relation by assuming uniform compression (i.e. larger values of ρ), while the small atomic separations found in liquid structures and in interstitials occur with very little change in ρ.

Examination of table 2 demonstrates that incorporating situations where small atomic separations occur into the fitting procedure leads to marked improvements in the melting point and latent heat and to small improvements in the change in density upon melting. Note that none of these properties was used in the fitting procedures. However, if desired, they could be incorporated. The technique for fitting ΔH_{melt} and ΔV_{melt} is straightforward and an approach to fitting the melting point was proposed by Sturgeon and Laird (2000).

Acknowledgements

The authors thank Professor W. Hoyer and Dr I. Kaban for providing the detailed experimental structure factor data for liquid iron used in the present work and to Dr M.I. Baskes for useful discussion. This research was supported by the US Department of Energy through grant DE-FG02-99ER45797 (Princeton team), grant DE-FG02-01ER45910 (Northwestern team) and its Computational Materials Science Network. This research made use of resources at the National Energy Research Scientific Computing Center, which is supported by the Office of Science of the US Department of Energy under contract DE-AC03-76SF00098.

APPENDIX A

§ A 1. Embedded-atom method potential forms

Here, we provide a more complete description of the functional forms of the potentials developed in this paper. Recall that the general forms of the potentials are given by equations (1)–(5). The pairwise term takes the following form:

$$\varphi(r) = \begin{cases} \dfrac{Z^2 q_{\mathrm{e}}^2}{r}\phi\left(\dfrac{r}{r_{\mathrm{s}}}\right) & \text{for } r < r_1, \\ \exp^{(B_0+B_1 r+B_2 r^2+B_3 r^3)} & \text{for } r_1 < r < r_2, \\ \displaystyle\sum_{k=1}^{n^{\varphi}} a_k^{\varphi}(r_k^{\varphi}-r)^3\theta(r_k^{\varphi}-r) & \text{for } r > r_2, \end{cases} \tag{A 1}$$

where Z is the atomic number, q_e is the charge on an electron, $\theta(x)$ is the Heaviside step function,

$$r_s = 0.885\,34\frac{r_B}{2^{1/2}Z^{1/3}}, \tag{A 2}$$

$$\phi(x) = 0.1818\exp^{(-3.2x)} + 0.5099\exp^{(-0.9423x)} + 0.2802\exp^{(-0.4029x)} + 0.028\,17\exp^{(-0.2016x)} \tag{A 3}$$

and r_B is the Bohr radius. A detailed explanation of the functional form used in equation (A1) can be found in the papers by Ackland *et al*. (1997) and Biersack and Ziegler (1982). The density function is written as a cubic spline:

$$\psi(r) = \sum_{k=1}^{n^\psi} a_k^\psi (r_k^\psi - r)^3 \theta(r_k^\psi - r) \tag{A 4}$$

and the embedding energy as

$$\Phi(\rho) = -\rho^{1/2} + a^\Phi \rho^2. \tag{A 5}$$

The coefficients for potentials 2 and 4 can be found in table A 1.

Table A 1. The parameters describing potentials 2 and 4 where all distances are expressed in Å and energies in eV.

	Value for the following potentials	
Parameter	Potential 2	Potential 4
r_1	1.00	0.90
r_2	2.00	1.95
B_0	6.426 526 057 634 8	14.996 917 289 290
B_1	1.790 048 852 428 6	−20.533 174 190 155
B_2	−4.510 831 672 980 7	14.002 591 780 752
B_3	1.086 619 937 330 6	−3.647 373 659 114 3
a_1^φ (r_1^φ)	—	195.923 228 539 94 (2.1)
a_2^φ (r_2^φ)	−24.028 204 854 115 (2.2)	17.516 698 453 315 (2.2)
a_3^φ (r_3^φ)	11.300 691 696 477 (2.3)	1.492 652 516 429 0 (2.3)
a_4^φ (r_4^φ)	5.314 449 582 046 2 (2.4)	6.412 947 612 519 7 (2.4)
a_5^φ (r_5^φ)	−4.665 953 285 604 9 (2.5)	−6.815 746 186 055 3 (2.5)
a_6^φ (r_6^φ)	5.963 775 852 919 4 (2.6)	9.658 258 196 360 0 (2.6)
a_7^φ (r_7^φ)	1.771 026 200 606 1 (2.7)	−5.341 900 276 441 9 (2.7)
a_8^φ (r_8^φ)	0.859 138 307 687 31 (2.8)	1.799 655 804 834 6 (2.8)
a_9^φ (r_9^φ)	−2.184 536 296 826 1 (3.0)	−1.478 896 663 628 8 (3.0)
a_{10}^φ (r_{10}^φ)	2.642 437 700 746 6 (3.3)	1.853 043 528 366 5 (3.3)
a_{11}^φ (r_{11}^φ)	−1.035 834 537 020 8 (3.7)	−0.641 643 448 593 16 (3.7)
a_{12}^φ (r_{12}^φ)	0.335 482 649 515 82 (4.2)	0.244 636 300 251 68 (4.2)
a_{13}^φ (r_{13}^φ)	−0.046 448 582 149 334 (4.7)	−0.057 721 650 527 383 (4.7)
a_{14}^φ (r_{14}^φ)	−0.007 029 496 304 868 9 (5.3)	0.023 358 616 514 826 (5.3)
a_{15}^φ (r_{15}^φ)	—	−0.009 .706 492 126 507 9 (6.0)
a_1^ψ (r_1^ψ)	11.686 859 407 970 (2.4)	11.686 859 407 970 (2.4)
a_2^ψ (r_2^ψ)	−0.014 710 740 098 830 (3.2)	−0.014 710 740 098 830 (3.2)
a_3^ψ (r_3^ψ)	0.471 935 270 759 43 (4.2)	0.471 935 270 759 43 (4.2)
a^Φ	−0.000 353 870 965 799 29	−0.000 349 061 783 635 30

References

Ackland, G. J., Bacon, D. J., Calder, A. F., and Harry, T., 1997, *Phil. Mag*. A, **75**, 713.
Baroni, S., Dal Corso, A., de Gironcoli, S., and Giannozzi, P., http://www.pwscf.org.
Baskes, M. I., 1992, *Phys. Rev*. B, **46**, 2727.
Biersack, J. P., and Ziegler, J. F., 1982, *Nucl. Instrum. Meth*., **141**, 93.
Car, R., and Parrinello, M., 1988, *Phys. Rev. Lett*., **60,** 204.
Carlsson, A. E., 1990, *Solid St. Phys*., **43**, 1.
Daw, M. S., and Baskes, M. I., 1984, *Phys. Rev*. B, **29**, 6443.
Domain, C., and Becquart, C. S., 2001, *Phys. Rev*. B, **65**, 024 103.
Ercolessi, F., and Adams, J. B., 1994, *Europhys. Lett*., **26**, 583.
Finnis, M. W., and Sinclair, J. E., 1984, *Phil. Mag*. A, **50,** 45.
Gardner, A. B., Sanders, A. L., and Slifkin, L. M., 1968, *Phys. Stat. sol*., **30**, 93.
Il'inskii, A., Slyusarenko, S., Slukhovskii, O., Kaban, I., and Hoyer, W., 2002, *Mater. Sci. Engng*, **A325**, 98.
Jacobsen, K. W., Norskov, N. K., and Puska, M. J., 1987, *Phys Rev*. B, **35**, 7423.
Johnson, R. A., 1964, *Phys. Rev*. A, **134**, 1329.
Lee, B. J., and Baskes, M. I., 2000, *Phys. Rev*. B, **62**, 8564.
Lee, B. J., Baskes, M. I., Kim, H., and Cho, Y. K., 2001, *Phys. Rev*. B, **64**, 184 102.
Mehl, M. J., and Papaconstantopoulos, D. A., 1996, *Phys. Rev*. B, **54**, 4519.
Mendelev, M. I., 1998a, *J. non-crystalline Solids*, **223**, 230; 1998b, *ibid*., **232–234**, 560; 1999, *Physica* B, **262**, 40.
Mendelev, M. I., and Srolovitz, D. J., 2002, *Phys. Rev*. B, **66**, 014 205.
Mermin, N. D., 1965, *Phys. Rev*. A, **137**, 1441.
Morris, J. R., Wang, C. Z., Ho, K. M., and Chan, C. T., 1994, *Phys. Rev*. B, **49**, 3109.
Morris, J. R., and Song, Z., 2002, *J. chem. Phys*., **116**, 9352.
Osetsky, Yu.N., Mikhin, A. G., and Serra, A., 1995, *Phil. Mag*. A, **72**, 361.
Pak, H. M., and Doyama, M., 1969, *J. Fac. Engng, Tokyo Univ*., B, **30**, 111.
Parinello, M., and Rahman, A., 1980, *Phys. Rev. Lett*., **45**, 1196; 1981, *J. appl. Phys*., **52**, 7182; 1982, *J. chem. Phys*., **76**, 2662.
Perdew, J. P., Burke, K., and Ernzerhof, M., 1996, *Phys. Rev. Lett*., **77**, 3865.
Rose, J. H., Smith, J. R., Guinea, F., and Ferrante, J., 1984, *Phys. Rev*. B, **29**, 2963.
Shewmon, P. G., 1963, *Diffusion in Solids* (New York: McGraw-Hill).
Sturgeon, J. B., and Laird, B. B., 2000, *Phys. Rev*. B, **62**, 14 720.
Vanderbilt, D., 1990, *Phys. Rev*. B, **41**, 7892.
Waseda, Y., 1980, *The Structure of Non-crystalline Materials* (New York: McGraw-Hill).